# Electrostatic gating and intercalation in 2D materials

*Yecun Wu*[1,2,6], *Danfeng Li*[1,3,4,6], *Chun-Lan Wu*[5,6], *Harold Y. Hwang*[1,3]✉ *and Yi Cui*[1,5]✉

Abstract | The doping or the alteration of crystals with guest species to obtain desired properties has long been a research frontier in materials science. However, the closely packed lattice structure in many crystals has limited the applicability of this strategy. The advent of 2D layered materials has led to revitalized interest in utilizing this approach through two important strategies, gating and intercalation, offering reversible modulation of the properties of the host material without breaking chemical bonds. In addition, these dynamically tunable techniques have enabled the synthesis of new hybrid materials. Here, we review how interactions between guest species and host 2D materials can tune the physics and chemistry of materials and discuss their remarkable potential for creating artificial materials and architectures beyond the reach of conventional methods.

The quest for materials by design has long motivated scientists to tailor materials to obtain desired functionalities. For centuries, various control and modulation tools have been developed to tune materials properties, for example via doping, phase control, defects and strain[1–5]. In the past few decades, the on-demand introduction of electrons, holes or ions into a host material for the purpose of engineering its electrical, optical and structural properties has been widely employed to enable revolutionary advances in semiconductor technology, giving rise to the concept of guest-species (atoms, ions, molecules) modification.

There are several key features of this modulation method that are inherent to the properties of the guest species. First, the electronic-structure degrees of freedom, made available through the incorporation of different elements, can induce a broad range of doping and distinct types of interactions within the material. Second, the dynamic and mobile nature of the guest species allows for reversible tuning. Third, topotactic transformations, which preserve the material's structural topology and take advantage of the imbalanced kinetic properties of different ion species, enable the synthesis of new materials with metastable lattice environments and valence states. More importantly, as discussed later in the text, building upon the intersection of chemical composition variations and electrostatic modulation (for example, with ionic tuning) substantially expands tunability beyond the limits of conventional approaches.

2D materials, especially 2D transition metal dichalcogenides (TMDs), as a large family with diverse physical properties and functionalities, have brought new vitality into this field, presenting a perfect platform for guest-species modification because of their confined, atomically thin layered structure[6–8]. 2D materials are suitable for guest-species intercalation because of their anisotropic bonding (covalent within the layer and van der Waals interactions between layers). The weak interlayer interaction facilitates the isolation of monolayer flakes, whose properties are extremely sensitive to changes in the surrounding environment. In addition, guest-species insertion into layered 2D materials can be achieved by accessing the van der Waals gap without breaking the intra-layer covalent bonds, maintaining the host structure of the 2D materials and confining the doped species[9]. These strategies constitute flexible pathways to synthesize novel materials systems by combining the diverse properties of the 2D materials and the guest species, leading to potential applications in quantum devices and energy[10–12].

Research on layered transition metal oxides, another heavily studied family of materials, has also flourished, motivated by the opportunities afforded by reduced dimensionality. Layered transition metal oxides attract much research interest owing to their sophisticated structural chemistry and the wide span of physical properties they display[13]. They often host many-body phenomena owing to the strong electronic correlations of the transition metal *d* orbitals and the entanglement between the charge, spin and lattice degrees of freedom, facilitated by the hybridization between transition metal cations and oxygen anions[14]. A defining consequence of these strong interactions is a broad range of functionalities, spanning from ferroic orders[15] to superconductivity[16]. The different energy landscapes present in the materials promote intertwined phases resulting in rich phase diagrams with competing orders and ground states, which are extremely sensitive to

[1]*Stanford Institute for Materials and Energy Sciences, SLAC National Accelerator Laboratory, Menlo Park, CA, USA.*

[2]*Department of Electrical Engineering, Stanford University, Stanford, CA, USA.*

[3]*Department of Applied Physics, Stanford University, Stanford, CA, USA.*

[4]*Department of Physics, City University of Hong Kong, Kowloon, Hong Kong SAR.*

[5]*Department of Materials Science and Engineering, Stanford University, Stanford, CA, USA.*

[6]*These authors contributed equally: Yecun Wu, Danfeng Li, Chun-Lan Wu.*

✉*e-mail: hyhwang@stanford.edu; yicui@stanford.edu*

https://doi.org/10.1038/s41578-022-00473-6

tuning parameters, from the transition metal oxidation state to the chemical environment[13,14,16]. For these reasons, the interaction between transition metal oxides and guest species has attracted enduring interest in materials synthesis research.

In this Review, we focus on guest-species tuning applied to 2D layered chalcogenides and oxides. We first introduce the two major techniques that can be used for guest-species tuning, electrostatic gating and intercalation. The mechanism and experimental design of each technique are briefly discussed. Then, we present the exciting progress enabled by guest-species modulation, covering both application-oriented work and the discovery of new phenomena. Finally, we provide an outlook on the immense possibilities offered by ionic tuning in 2D layered chalcogenides and oxides, and the perspectives for the extension of this methodology to other materials families.

Traditional guest-species tuning of 3D materials (FIG. 1a) is mainly dependent on chemical reactions between host materials and guest ions, introduced into the host material electrons and holes as donors and acceptors, respectively, which form covalent bonding with surrounding atoms (FIG. 1b). The insertion of guest species into the host material inevitably introduces defects and structural deformation. Instead, because of the layered and thin nature of the 2D materials, two new types of interactions, that do not disrupt the existing covalent bonds, can be obtained: the guest species can reside on the atomic surface and polarize the 2D material (gating; FIG. 1c), or the ions can migrate into the interlayer sites and chemically interact with the material (intercalation; FIG. 1d).

## Guest-species gating

Guest-species gating works in a similar way to the tuning of metal–oxide–semiconductor field-effect transistors (MOSFETs), by shifting the chemical potential of the material that acts as the channel in the transistor device[1,17]. A dielectric is required in both cases to provide the capacitance that holds the charges induced by an external voltage source, but the nature of the dielectric component is different in ionic gating and conventional oxide-based transistor gating. In MOSFETs, the dielectric is usually an insulating oxide layer, most commonly $SiO_2$, with a thickness ranging from tens to hundreds of nanometres (FIG. 2a). For guest-species gating, a medium composed of mobile ions, an electrolyte, is between the gate electrode and the channel. For this reason, guest-species gating is also known as ionic gating. The formation of an electrical double layer (EDL) at the interface between the electrode and the electrolyte induces an EDL capacitance that is much higher than the capacitance of oxide dielectrics[18].

A double layer is a universal phenomenon observed at electrode–electrolyte interfaces and is manifested as two layers of excess charges with opposite signs, one in the electrode and one in the electrolyte. Owing to the requirement of global charge neutrality, the double layer forms following the abrupt change in the interatomic force experienced by the ions at the interface between the bulk of the electrolyte and the electrode. In particular, ions close to the electrode experience very different forces from the electrode and the electrolyte and rearrange accordingly, forming a charged layer in the electrolyte. Owing to the Coulomb force exerted by this charged layer, the mobile electrons in the electrode are either accumulated or depleted at the interface to balance these excess net charges. Consequently, a layer of charges with opposite sign forms in the electrode. When the electrode is connected to an external voltage source, the density and polarity of the charges in the double layer can be conveniently controlled. The double layer is effectively a capacitor with a thickness of 1 nm or less at reasonable electrolyte concentrations, resulting in an ultra-high capacitance[19]. In this regard, an additional differential capacitance ($C = d\sigma/d\Psi$) can be used to describe the change of surface charge density ($\sigma$) with respect to the electric surface potential ($\Psi$). To build a transistor, a second electrode — the gate electrode — is put into the electrolyte and connected to a power source (FIG. 2b). An external voltage applied at the electrode relative to the channel translates to drops in voltage within the double layers at the electrolyte–gate electrode and electrolyte–channel interfaces. Because of the ultra-high capacitance of the double layer, a high 2D carrier density (up to $10^{14}\,cm^{-2}$) can be induced in the channel at a reasonably low gate voltage. Transistors based on this principle are termed electric double-layer transistors (EDLTs), and have been demonstrated with both liquid and solid-state ionic gates[20,21]. Beyond the gating effect, electrochemical reactions such as intercalation can also be observed in EDLTs. The gating effect and electrochemical reactions do not occur simultaneously: a lower gate voltage leads to the gating effect whereas a higher voltage leads to electrochemical reactions.

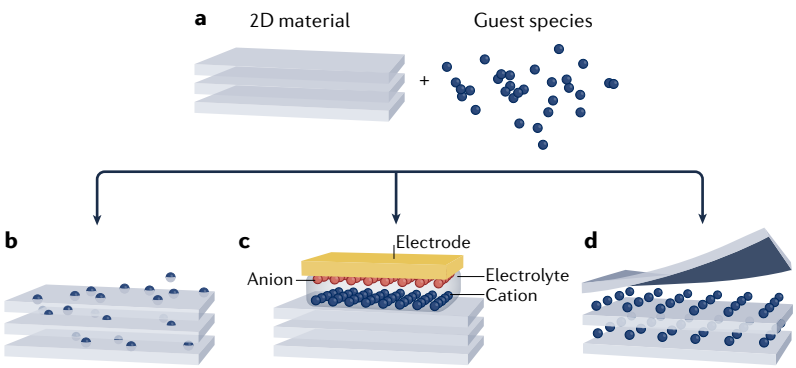


Fig. 1 | **Interactions between 2D materials and guest species. a** | A 2D material and guest species. **b** | Guest-species substitutional doping of a 2D material. **c** | Guest-species gating of a 2D material. **d** | Guest-species intercalation of a 2D material.

### *Liquid, gel and polymer-based electrolytes*

Commonly used electrolytes that have long been utilized in electrochemical devices include ionic liquids and lithium ion-based electrolytes (FIG. 2b). Ionic liquids are a family of salts that have a low melting point and are in liquid form at room temperature[22,23]. These electrolytes exhibit an area capacitance that can reach tens of microfarads per square centimetre, and have been employed to induce ambipolar conduction[20,24–26] and superconductivity[27–29] in a wide range of 2D materials. $Li^+$-based electrolytes are a critical component in rechargeable lithium batteries and are also widely used

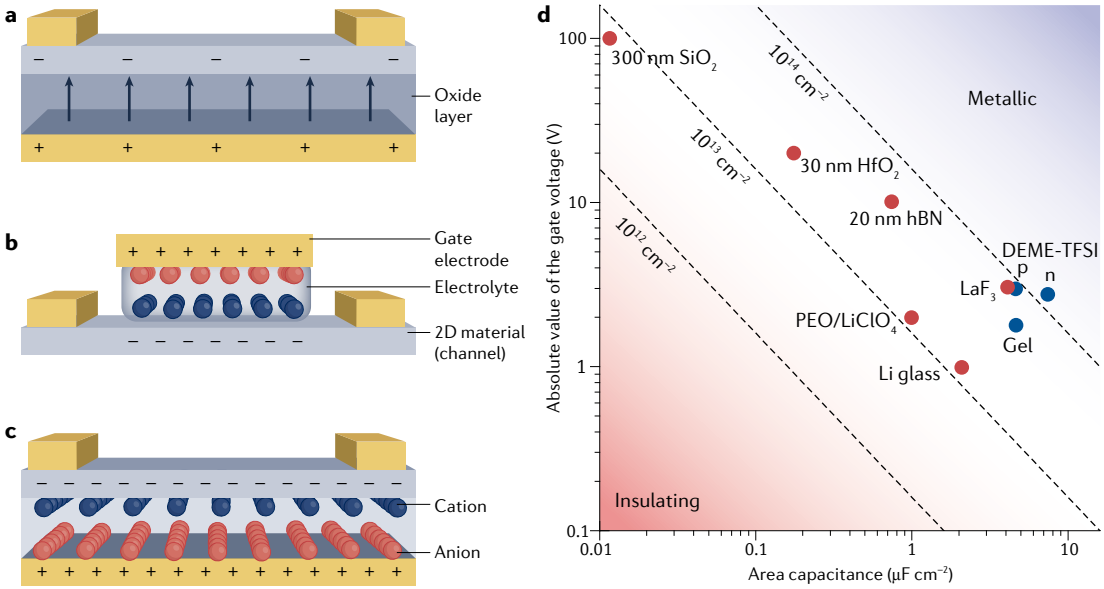


Fig. 2 | **Guest-species gating method. a–c** | A conventional dielectric oxide gate (part **a**), an ionic liquid gate (part **b**) and a solid-state ionic gate (part **c**). Arrows in part **a** represent the dielectric polarization direction. Blue and red spheres represent positively and negatively charged guest species. **d** | Area capacitance and the corresponding absolute values of the gate voltages that can be applied. Capacitance values of solid-state dielectrics are calculated by a parallel-plate capacitor model: $C_g = (\varepsilon_0 \times \varepsilon_d)/d_d$, where $\varepsilon_0$ is the relative permittivity of free space, $\varepsilon_d$ is the out-of-plane dielectric constant for dielectrics[43,199] and $d_d$ is the thickness of the dielectrics. Capacitance values of ionic gates are obtained from the literature[20,21,32,33,40]. Solid-state electrolytes are represented by red dots, whereas liquid or gel electrolytes are represented by blue dots. Product of the area capacitance and gate voltage indicates the surface doping concentration (dashed lines). Regions of the plot corresponding to carrier densities resulting in a metallic and insulating behaviour are shaded blue and red, respectively. DEME-TFSI, diethylmethyl(2-methoxyethyl)ammonium bis(trifluoromethylsulfonyl)imide; hBN, hexagonal boron nitride; $LiClO_4$, lithium perchlorate; PEO, poly(ethylene oxide).

in EDTLs. For EDLT fabrication and measurements, electrolytes consisting of lithium salts dissolved in an organic solvent or a polymer matrix are commonly used[25,30–32]. Another widely used gating technique is gel gating. The high viscosity of gel-based electrolytes translates to better mechanical integrity and lower evaporation rates compared with liquid-based electrolytes, making them easier to handle and more compatible with long electrical measurements[33,34].

Despite the broad tunability of liquid, gel and polymer electrolytes, there are some intrinsic issues complicating their use. One significant drawback is the unwanted strain created because of the glass transition of the electrolyte when the temperature is lowered, which is detrimental during low-temperature transport measurements[35]. Other issues include instability against moisture and undesirable side chemical reactions. The former can lead to the degradation of device performance at ambient conditions due to water absorption, whereas the latter are unavoidable at high bias in all EDLTs and lead to a behaviour analogous to electrical breakdown in oxide dielectric-based transistors. Nevertheless, these undesirable electrochemical reactions usually occur after the materials properties have already been tuned to a large extent, so that they remain largely unaffected.

### *Solid ceramic-based electrolytes*

Solid-state ionic gating has been developed to tackle some of the issues of liquid and gel electrolytes (FIG. 2c). Early developments involved the use of porous oxide as a solid-state proton gate based on the proton $H^+$ hopping mechanism[36–38]. However, the proton conductivity in porous oxides is highly dependent on the humidity of the environment, which makes integration with current solid-state semiconductor technology and packaging difficult. Starting from 2016, ceramic-based electrolytes have been used to fabricate EDLTs. These electrolytes include lithium-ion conductive glass ceramics[39,40], sodium superionic conductors[41] and fluoride-ion superionic conductors ($LaF_3$)[21]. There are several advantages of using these ceramic-based electrolytes for gating. First, strain degradation of device integrity can be significantly reduced for low-temperature experiments, owing to the absence of a glass transition in these electrolytes. Second, the mechanical rigidity of the electrolyte enables its use as both the gate dielectric and the substrate, which leads to a more integrated device architecture and enables further device processing after EDLT measurements. Third, the solid-state gate allows back gate geometries (FIG. 2c), leaving the top surface of the channel material accessible to be studied with surface-sensitive experimental techniques and advanced spectroscopic measurements. For example, the optical absorption spectrum of the electrolyte itself is a critical factor for experimental design. However, commonly used ionic liquids show strong absorption in the infrared spectrum[42], which inhibits spectroscopic investigations of the intrinsic materials properties in this energy spectrum. Finally, because they do not outgas, solid-state EDLTs are compatible with ultra-high vacuum measurements. Therefore, there is a

lot of potential for these devices to be integrated with a wide range of in situ vacuum-assisted materials synthesis and/or synchrotron-based measurements.

### *Effects of gating*

The performance of devices based on various electrolytes, in terms of area capacitance and absolute value of the corresponding maximum gate voltage[20,21,32,33,40,43], is compared in FIG. 2d. The maximum value of the applied gate voltage in solid-state dielectrics is bounded by the dielectric breakdown voltage[44], whereas for ionic electrolytes this breakdown occurs at voltages high enough to trigger certain electrochemical reactions, such as the electrolysis of the electrolyte or intercalation of the ions. The maximum carrier density variation induced by gating can be calculated as the product of the area capacitance and maximum gate voltage. Usually, 2D materials with a carrier density lower than $10^{11}$ cm$^{-2}$ are considered insulators. An insulator to metal transition occurs when the carrier density exceeds ~$10^{13}$ cm$^{-2}$. At a considerably high carrier density (>$10^{14}$ cm$^{-2}$), novel phenomena start to emerge, such as superconductivity or quantum phase transitions, as discussed later. As a comparison, solid-state dielectrics with a high dielectric constant, $\kappa$, can be used to achieve a carrier density around $10^{13}$ cm$^{-2}$ with a high ON/OFF ratio (for example, up to $10^8$ in a $HfO_2$-based transistor[43]; FIG. 2d), making them desirable for CMOS-like digital logic devices and allowing reduction of the channel length[43,45,46]. However, because of dielectric breakdown[44], reaching higher doping concentrations electrostatically using solid-state dielectrics is still challenging. One of the most distinctive aspects of guest-species gating is the extremely high capacitance that can be reached (FIG. 2d), which can surpass that of traditional solid-state gate dielectrics by one to three orders of magnitude. For a FET device based on guest-species gating, this leads to a low threshold voltage and steep subthreshold slope in the current–voltage characteristic. As a consequence, the 2D materials can be highly doped, reaching carrier densities of ~$10^{14}$ cm$^{-2}$ (FIG. 2d). The first generation of transistors based on ionic liquid gates suffered from issues such as low ON/OFF ratios (~200), which was probably due to a non-zero 'OFF' state current passing through the interior of the crystal beneath the channel surface[20]. To circumvent this problem, liquid gating strategies including dual-gate or suspended configurations have been developed to improve the ON/OFF ratio to more than $10^5$. Alternatively, solid-state ionic conductors, despite having a slightly smaller area capacitance than the liquid gate, show some promise because of their low leakage current and high integrability. However, the technical development of solid-state ionic gates is still in the early stages.

The high doping concentrations that can be reached using guest-species gating have engendered novel phenomena. One remarkable development was the superconductivity and ground-state tuning induced in TMD-based band insulators by interaction with guest species[47]. For instance, gating suspended $MoS_2$ bilayers using ionic liquid gate electrodes led to the emergence of superconductivity in atomic sheets and controllable Josephson coupling between the layers[48] (FIG. 3a). More specifically, a double-side gate structure, obtained by immersing suspended samples in ionic liquid to accumulate ions on both top and bottom layers, resulted in a stronger gate effect than a single-side gate[48]. Moreover, by varying carrier density in 2D superconductor ZrNCl, large and overlapping electron pairs, in the Bardeen–Cooper–Schrieffer limit, could be tuned to small and tightly bound electron pairs, leading to Bose–Einstein condensation[49]. In addition, the emergence of collective many-body states induced by ionic gating in $TiSe_2$, leading to superconducting and CDW phases, has also been reported[50] (FIG. 3b). Beyond doping, an electrochemical reaction under high gate voltage was used to electrochemically etch the layered superconductor FeSe, revealing superconducting behaviour and enabling its tuning in devices down to the monolayer level[51].

Another thriving field is the research on gate control of 2D magnetism. A room-temperature 2D ferromagnet was achieved by lithium-ion gating of trilayer $Fe_3GeTe_2$ (FIG. 3c); the elevated Curie temperature was attributed to the substantial shift of the electronic bands of $Fe_3GeTe_2$ induced by ionic gating[52]. In $Cr_2Ge_2Te_6$, the scale of the magnetization hysteresis was found to be much larger when using ionic gating than silicon gating[53]. More recently, tuning of the magnetic anisotropy was demonstrated in this material. The out-of-plane easy axis of pristine $Cr_2Ge_2Te_6$ was switched to in-plane under heavy electron doping due to the electron-induced sign change of the magnetic anisotropy energy[54] (FIG. 3d).

Phase control of 2D materials was also observed. Semiconductor to semimetal phase transitions in group VIB TMDs caused by the change in electron chemical potential at high doping concentration were first predicted by theory[55] and later observed in experiments[56,57] (FIG. 3e). The guest-species gating method was also applied to photonic devices. In a monolayer $WS_2$-based resonator, the large change in the refractive index and the minimal change in the imaginary response induced by ionic gating were exploited to fabricate an efficient phase modulator[58] (FIG. 3f). Notably, in some studies, especially when using lithium ion-based ionic gates[30,49,52], the doping at high gate voltage was caused by intercalation rather than electrostatic gating, which will be discussed later.

Finally, ionic conductivity is a key parameter for ionic gating techniques. The slow movement of the ionic guest species requires low bias scan rates to maintain equilibrium at the gate–channel interface, especially at low temperature[59]. Therefore, there is strong interest in developing gating methods with high ionic conductivity for high-speed or high-frequency response. However, the slow dynamics at low temperature can also be exploited. Ionic liquid-induced doping can be non-volatile at low temperatures due to the freezing of the guest species[60]. For example, by utilizing the temperature-induced transition between ionic insulating and conducting states in AgI, a solid-state non-volatile doping approach for 2D semiconductors — leading to devices operational at room temperature and programmable between 100 °C and 175 °C — was demonstrated. This method allows the fabrication of reversibly programmable devices that can

function as transistors or diodes with switchable carrier types or device polarities[61].

## Guest-species intercalation

In addition to gating methods where guest species are on the surface of the 2D materials, the weak interlayer interaction of 2D materials permits the insertion of guest species into the interlayer spacing in an ordered pattern. Three different guest species can be intercalated into 2D materials: atoms, ions and molecules.

Atoms are intercalants in their zero-valent states. Transition metals such as copper, cobalt, silver or gold can usually be intercalated into layered materials while preserving their zero-valent state[62–64], which is usually a result of a low level of electron exchange between the host material and the intercalant, and a weak interlayer interaction.

Ions are intercalants with net electrical charges. Cations, including most of the alkali metals (lithium, sodium, potassium and so on), some transition metals (chromium, iron, nickel and so on)[65,66] and rare earth metals (scandium, neodymium, europium and so on)[67], can be intercalated at or de-intercalated from their valence states into the host materials. Non-metal ions such as oxygen ions can also be intercalated[68], especially in 2D layered oxides[69]. Ion intercalation and insertion normally triggers changes in coordination number and crystal-field environment. Theoretical calculations show that the bonding between lithium ions and a graphite lattice has a covalent character[70]. Transition metal ions

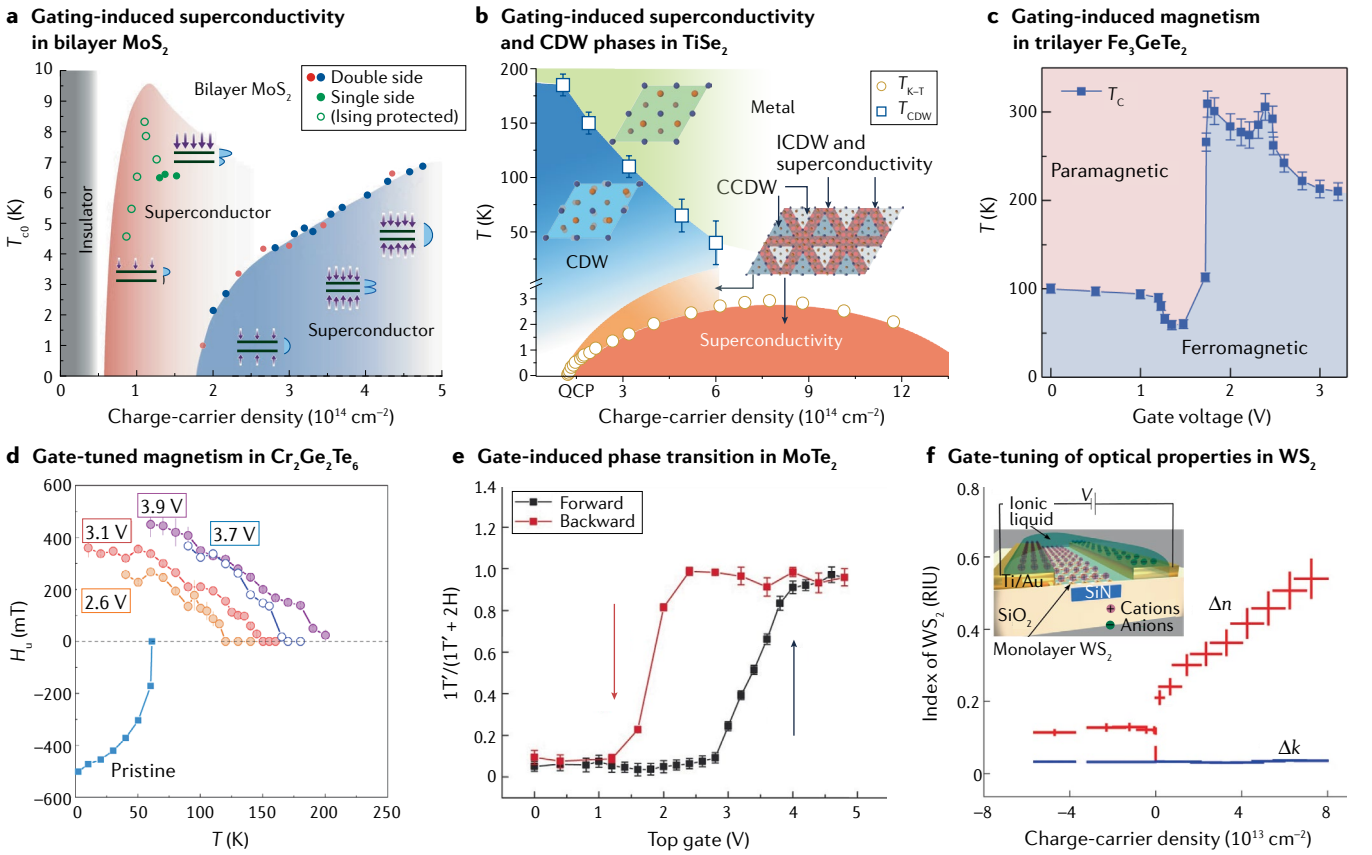


Fig. 3 | **Gate-controlled modulation and phase diagrams in 2D materials.** **a** | Superconducting phase diagram for ionic gated bilayer $MoS_2$ devices, showing one single-side gate and two double-side gates, as indicated by the arrows. Onsets of superconductivity are close to a carrier density of $n_{2D} = 0.6 \times 10^{14}\ cm^{-2}$ for the single-side device and of $1.8 \times 10^{14}\ cm^{-2}$ for the double-side devices[48]. $T_{c0}$ is defined as the transition temperature at which the resistance reaches 50% of the normal resistance. Ising protected means a coupled superconducting state with strong Ising-type spin–orbit coupling. **b** | Phase diagram of 1T-$TiSe_2$ under electron doping through ionic gating, showing the control obtained over the charge-density wave (CDW) transition temperature ($T_{CDW}$) and over the superconductivity transition temperature ($T_{K–T}$, the Kosterlitz–Thouless-type transition temperature)[50]. **c** | Phase diagram of a trilayer $Fe_3GeTe_2$ sample as the gate voltage and temperature are varied[52]. **d** | Uniaxial magnetic anisotropy fields of $Cr_2Ge_2Te_6$ as a function of temperature for different values of the gate bias[54]. The magnetic easy axis of pristine $Cr_2Ge_2Te_6$ is in the out-of-plane direction ($H_u < 0$), whereas the in-plane spin orientation is more stable in gated $Cr_2Ge_2Te_6$ ($H_u > 0$). **e** | Raman intensity showing a gate-controlled structural transition between the 1T′ and 2H phases of $MoTe_2$ (REF.[56]). The intensity ratio $F = 1T'(A_g) / [1T'(A_g) + 2H(A_1')]$ represents the fraction of 1T′ phase in the sample, where $A_g$ and $A_1'$ represent the $A_g$ Raman mode of 1T′ phase $MoTe_2$ and the $A_1'$ Raman mode of 2H phase $MoTe_2$, respectively. Black and red curves show increasing and decreasing gate voltage, respectively. The hysteresis of the Raman intensity ratio versus gate voltage indicates a gate-controlled structural transition of $MoTe_2$ between 2H and 1T′ phases. **f** | Change in the real and imaginary parts of the refractive index of monolayer $WS_2$ ($\Delta n$ and $\Delta k$) with gate-induced carrier density. The schematic shows the composite SiN–$WS_2$ waveguide with the ionic liquid on top[58]. CCDW, commensurate CDW; ICDW, incommensurate CDW; QCP, quantum critical point; RIU, refractive index unit; $T_C$, Curie temperature. Panel **a** reprinted from REF.[48], Springer Nature Limited. Red shaded region in panel **a** reproduced with permission from REF.[27], AAAS. Panel **b** reprinted from REF.[50], Springer Nature Limited. Panel **c** adapted from REF.[52], Springer Nature Limited. Panel **d** reprinted from REF.[54], Springer Nature Limited. Panel **e** reprinted from REF.[56], Springer Nature Limited. Panel **f** adapted from REF.[58], Springer Nature Limited.

in TMDs are usually covalently bonded with the coordinated host atoms[71]. After ion intercalation, the weak interlayer van der Waals interactions are replaced by strong Coulomb interactions, for alkali metals, or covalent interactions, for covalent metal ions[9].

Molecules, both organic and inorganic, can also act as intercalants. In particular, nitrogen-containing organic molecules of various sizes, from several angstroms to a few nanometres, can be intercalated[72]. Two major inorganic intercalants are metal hydroxides[73] and metal halides[74].

To insert guest species in a layered 2D material, the intercalated compound must be, under the given experimental conditions, thermodynamically more stable than the physical mixture of the 2D material and the guest species; otherwise, deposition will occur rather than intercalation. The kinetics of the intercalation process depends on the spacing or the van der Waals gap of the 2D material[75], the existence of surface defects and the diffusion coefficients of the guest species between sites within the spacing[76]. In the case of zero-valent intercalants, because they do not change the oxidation state of the host lattice, high concentrations of intercalated species can be obtained, depending on the concentration of the precursor salt solution and the crystal structure of the host[77]. In intercalated compounds, the stability of intermediate or end phases is influenced by the type of species inserted and the extent of intercalation[78]. We now discuss different methods to achieve guest-species insertion, with a particular focus on topochemical methods.

### *Solid-state reactions*

Solid-state reactions usually refer to direct reactions of 2D materials and intercalants at elevated temperatures. High temperatures are generally required due to the large energetic barriers for the diffusing species. In certain temperature regimes, various competing chemical reactions can be energetically accessible, resulting in the formation of different thermodynamically stable phases. Such high-temperature reaction methods have been widely used for the incorporation of transition metals. Examples include the intercalation of metal ions[79] and molecules such as organic molecules[72] or metal halides[74] into group IVB and group VB TMDs or graphite. This method has also been employed for the synthesis of specific transition metal oxides[80]. In general, for these materials, different thermodynamically stable phases or mixtures of these phases can be produced. The high-temperature synthetic routes represent 'thermodynamic control' and are generally restricted to the formation of only the most thermodynamically stable phase(s) for a specific composition, which precludes the formation of a large number of metastable materials.

### *Electrochemical reactions*

In the electrochemical approach, the intercalation process is facilitated by the inclusion of a power source, which serves as an external knob to control the reaction. The electrochemical intercalation process requires an electrochemical device consisting of three critical components: the targeted host material, which serves as the working electrode; an electrolyte or molten salt containing the ionic intercalants and with an adequately high ionic conductivity for ion transport; and a counter electrode where an electrochemical reaction can be established to complete the electrical circuit. The intercalation process can be driven by controlling either the current passing through the circuit or the voltage applied across the two electrodes[81]. A crucial prerequisite is that the intercalants, electrolyte and host 2D material are electrochemically stable within the applied voltage window. The electrochemical approach enables the control of the intercalation rate by following the voltage profile, so that the degree of intercalation, or the number of ions intercalated, can be monitored[82–84]. To this end, the correlation between the intercalation time and the number of ions intercalated enables the systematic modulation of the carrier density in the host materials[85]. Additionally, this process is highly reversible unless the voltage is so high that it induces a phase transition. For example, lithium intercalation in $LiCoO_2$ is highly reversible when the charging voltage is below 4.2 V (REF.[86]). However, at high charging voltages, an irreversible phase transition occurs due to degradation by oxygen release[87,88]. Within the appropriate voltage window, intercalation by electrochemical means constitutes a powerful reversible method for both ionic and electronic tuning of materials[89].

### *Topochemical reactions*

Intercalation can also be achieved at low temperatures topochemically by leveraging large differences in the kinetics of the diffusing ions, especially in complex layered materials, leading to the synthesis of novel metastable phases[90,91]. Certain groups of atoms and ions can become, for a given chemical environment and temperature, significantly more mobile than the host phase in which they reside. Using this phenomenon as the driving force, these atoms or ions can be effectively inserted into, or removed from, the host phases, forming new metastable phases or novel structures, provided that these species possess large mobility in the host lattice and/or that the host phases have a tendency to be reduced or oxidized. By carefully choosing the initial phases, topochemical reactions can facilitate the formation of a wide range of end phases that are usually inaccessible via high-temperature synthetic routes. The topochemical method is widely used for the intercalation of atoms and ions, and specifically oxygen de-intercalation in transition metal oxides.

***Atom and ion intercalation.*** Chemical intercalation of atoms and ions is usually a solution-based process involving spontaneous or low-temperature heat-assisted redox reactions. Precursors containing the target ionic intercalants are dissolved in a solvent. The host material is then immersed in the solution for a period of time determined by the reaction kinetics and, if required, high temperature is applied to drive the reaction. Alkali metal ions have been chemically intercalated into various transition metal-based layered materials owing to the high reduction potential of the alkali metal precursors such as *n*-Butyllithium[92]. In recent years, a solution-based

zero-valent intercalation method has also been developed, in which the atoms in the solution can enter the 2D materials spontaneously due to a strong thermodynamic driving force[62]. Various charge-neutral metal atoms can be intercalated upon diffusion, driven by the local concentration gradient[63]. Many TMDs and oxides have been chemically intercalated with different guest species, such as $TaS_2$ (REF.[93]), GaSe[94], $Bi_2Se_3$ (REF.[62]), layered binary oxides and perovskite-derived oxides such as $WO_3$-type (REF.[95]), $MO_2$ rutile-type (for example, M = Mo, Mn)[96,97] and $AB_2O_4$ spinel-type oxides (for example, A = Li, and B = Mn, Ti)[98–100].

***Ion exchange.*** For ion-intercalated compounds, selective ion exchange can be promoted in an ionic environment by leveraging the difference in reduction or oxidation potential between the ions inside and outside the host 2D materials. For example, lithium-intercalated $MoS_2$ possesses a strong reduction capability. Through an ion exchange process involving lithium-intercalated $MoS_2$ and transition metal or rare earth metal salts, novel intercalation compounds of $MoS_2$ and transition or rare earth metals can be prepared[101]. Notably, this method was extended to noble metals (such as platinum) for the synthesis of high-performance catalysts[102,103]. Progress has also been made in the realization of ultra-fast ion diffusion enabled by exchanged ions in atomically thin mica, the exchanged ions forming island patterns in the mica with dimensions controlled by Moiré superlattice length scales[104].

***Oxygen de-intercalation.*** Unlike cation de-intercalation discussed above, which is usually achieved via electrochemical and solution-based chemical methods[62], oxygen de-intercalation often involves other reducing reagents, such as hydrogen[105–107], metal getters[108] and metal hydrides[109–114]. Hydrogen and metal getters need to operate at a relatively high temperature, usually above 300 °C, as a considerable amount of thermal energy is still required to facilitate oxygen release. At the required elevated temperatures, the formation of some metastable phases is precluded, and the reduction reactions typically lead to decomposition to binary oxide phases, rather than the targeted reduced phases[113]. To circumvent this issue, metal-based hydrides have been adopted as solid-state reducing reagents, with which the topochemical reactions can be operated at relatively low temperatures, thus preventing materials decomposition. These metal hydrides include NaH[109], LiH[115], $CaH_2$ (REFS.[110,111,114]) and $TiH_2$ (REF.[116]).

Numerous complex oxides, especially those with perovskite or perovskite-derived structures[91], are suitable precursors for topochemical transitions using metal hydrides. As a result, novel phases with unconventional transition metal oxidation states and coordination numbers can be produced[113]. Among the different possible topochemical transitions, the transition to the infinite-layer phase $ABO_2$ — where A is usually a bivalent or trivalent cation — with a square planar coordination to the transition metal ion (B) is one of the most studied oxygen de-intercalation processes[91]. Taking $SrFeO_x$ as an example, the formation of the $SrFeO_2$ infinite-layer phase can be readily facilitated using a $CaH_2$-based topochemical reduction from the precursor brownmillerite phase $SrFeO_{2.5}$ (REFS.[112,117]). This new phase cannot be directly synthesized by conventional high-temperature synthesis and shows a unique antiferromagnetic ground state, which can be converted into a $S = 1$ high-spin state with an antiferromagnetic to ferromagnetic transition upon applying pressure[118]. In general, imposing epitaxial strain by applying pressure in thin films represents an additional tuning knob to induce phase transitions that are inaccessible in bulk[119,120].

Another prominent example of oxygen de-intercalated oxides are Ruddlesden–Popper nickel oxides (nickelates) with low nickel valence, such as $La_3Ni_2O_6$ (REF.[121]) and $RE_4Ni_3O_8$, where RE can be lanthanum, praseodymium or neodymium[107,122–125], which can be prepared by oxygen de-intercalation using various reducing reagents. These layered compounds, long thought to be close cousins of copper oxide high-temperature superconductors[126], were found to present intriguing physics, including large orbital polarization, charge or spin ordering and stripe phases[107,124,125]. They recently attracted significant research interest due to their potential for developing high-temperature nickelate superconductors[126–128].

### *Effects of intercalation*

There are two major effects of intercalation on the chemical environment in materials. The first is doping. Unlike the gate-induced electrostatic doping in 2D materials, the intercalation-induced doping derives from charge transfer processes that require a difference in the chemical potential of the host 2D material and the intercalant and the availability of an empty band that accepts electrons or holes (FIG. 4a,b). The lithium ion, which possesses a very high reduction potential, is one of the most effective electron donors and can donate up to one electron per atom to the host lattice. Amphoteric 2D materials such as graphene can either be an electron acceptor or a donor during the intercalation process. For example, halogen intercalation in graphene has shown strong hole-doping behaviour[129,130]. However, most of the TMDs and oxides can only be electron acceptors during intercalation. This may be due to the bonding between the transition metal and chalcogens or oxygens that leads to a negatively charged chalcogen or oxygen layer[131]. As a consequence, the Coulomb repulsion between the layers and the negatively charged guest species may exceed the energy to be gained by intercalation[79]. Electronically, the topology of the Fermi surface of 2D materials can be largely controlled by doping.

The second effect is chemical bonding. The unique degree of freedom associated with the bonding configuration of the intercalants can lead to changes in the electronic structures of the intercalated compounds. Chemical bonds form when the valence electrons of the intercalant and host atoms interact with each other[71]. The difference in the electronegativity of these atoms affects the overlap of the electron clouds (FIG. 4c). Consequently, the electronic band structure is amenable to modifications by the formation of new chemical bonds or hybridization. The guest species can also replace the host atoms, modifying the lattice configuration[132]. For an

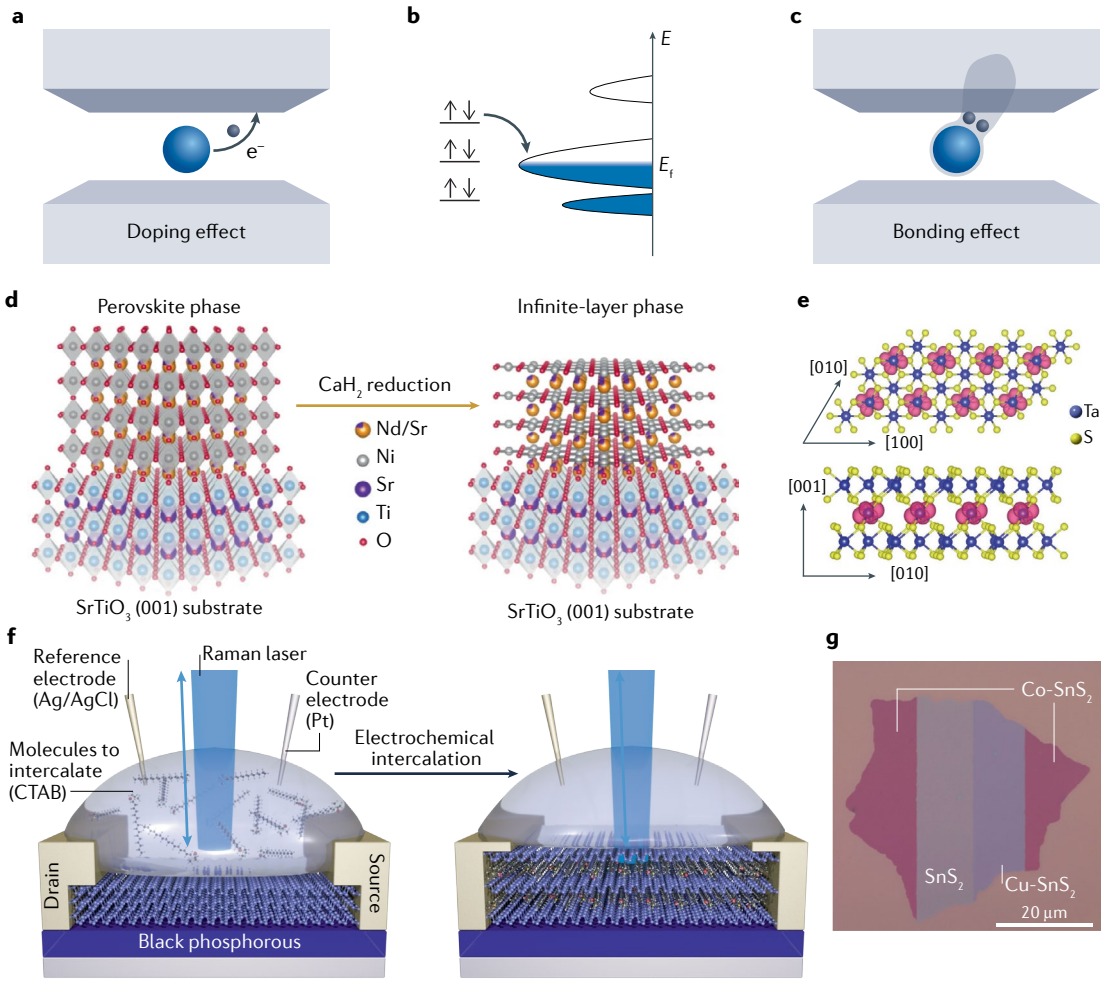


Fig. 4 | **Effects and progress of (de-)intercalation. a**,**b** | Schematic (part **a**) and band diagram (part **b**) of the charge transfer process-induced doping effect. **c** | Chemical bonding formation between the intercalant and the host 2D material. **d** | Oxygen de-intercalation process transforming a $Nd_{0.8}Sr_{0.2}NiO_3$ thin film with perovskite structure to a $Nd_{0.8}Sr_{0.2}NiO_2$ film with an infinite-layer structure[127]. **e** | Top view (top) and side view (bottom) spin density isosurface of tantalum-intercalated $Ta_7S_{12}$, showing that the intercalated tantalum atoms exhibit a net spin density[71]. **f** | A platform for the electrochemical intercalation of black phosphorus to obtain a monolayer atomic crystal molecular superlattice. The intercalation process can be monitored in situ using Raman spectroscopy[171]. **g** | Optical microscopy image demonstrating the seamless integration of $SnS_2$, Cu-$SnS_2$ and Co-$SnS_2$ within a single piece of nanosheet, the colours of the crystal strongly depending on the species of the intercalatant[179]. CTAB, cetyl-trimethylammonium bromide. Panel **d** reprinted from REF.[127], Springer Nature Limited. Panel **e** reprinted from REF.[71], Springer Nature Limited. Panel **f** reprinted from REF.[171], Springer Nature Limited. Panel **g** reprinted from REF.[179], Springer Nature Limited.

individual intercalant, these effects often coexist, leading to exotic phases and unusual electronic phenomena and motivating the development of novel applications.

***Superconductivity and electronic phase transition.*** Topochemical transformations enabled by intercalation can lead to new electronic parent phases that, upon doping, can become superconducting or reveal additional quantum states. These exotic phases are often a consequence of structural phase transitions, as discussed above. Doping achieved by intercalation or chemical substitution further modifies the band structure and/or electronic interactions with the host species, marked by free charges introduced into the material. In this regard, both the bonding and doping effects contribute to the creation of unconventional superconductivity and other related phases in 2D intercalated compounds.

The chemistry of cation de-intercalation in transition metal oxides involving monovalent cations such as lithium, sodium or potassium has been deeply investigated, as this process is generally the chemical reaction used in the charging of lithium-ion batteries. One prominent example is the various phases that can be prepared via de-intercalation of sodium ions from $NaCoO_2$, leading to $Na_xCoO_2$ compounds. $Na_xCoO_2$ has many polymorphs[133,134] that possess similar formation energy and can be synthesized through chemical and electrochemical oxidation, with the γ-$Na_xCoO_2$ phase the most studied compound[135]. The γ-$Na_xCoO_2$ phase is most stable when $x = 0.7$ (REF.[136]), but can be further de-intercalated to phases with $x < 0.5$ (REFS.[135,137,138]). Upon varying $x$ by de-intercalation, $Na_xCoO_2$ displays many exotic phases, evolving from a Curie–Weiss metal to a paramagnetic metal, and from a charge-density

wave (CDW) metallic state to a charge-ordered insulator, which leads to an intriguing phase diagram[138,139]. Surprisingly, when this system undergoes another intercalation process via the insertion of water molecules into the interlayer sites of edge-sharing $CoO_2$ pyramids, superconductivity emerges[140] and a superconducting dome appears in the phase diagram upon varying $x$[141–145]. Superconductivity in this layered system attracted immense interest not only due to a $Co^{3+}/Co^{4+}$-derived low spin to high spin transition[146–148] but also because of the inherent frustrated spin structure in the underlying triangular lattice of cobalt sites[139].

Infinite-layer nickelates with chemical formula $RENiO_2$, where RE is a rare earth element, represent another interesting materials family. The implementation of a metal hydride-based kinetic soft-chemistry approach enables the preparation of a metastable nickelate phase with an unusual nickel valence in both powder and thin-film forms[109–111,114,149,150]. This phase cannot be obtained by conventional high-temperature thin-film growth, and mimics the starting electronic structure of the superconducting copper oxides. Materials design exploiting this specific synthetic approach in combination with another type of ionic modification, chemical substitution, has been fuelled by the recent discovery of the first nickelate superconductor with an infinite-layer structure, thin-film $Nd_{1-x}Sr_xNiO_2$ (REF.[127]) (FIG. 4d) and its intriguing phase diagram[151,152]. The subsequent discovery of thin-film $Pr_{1-x}Sr_xNiO_2$ superconductors[153] hinted at the existence of an extended family of layered nickelate superconductors[154]. Furthermore, in particular for thin-film $RENiO_2$, the underlying substrate provides a template not only for hosting topotactically transformed single-crystalline films[151,152] but also for reorienting the oxygen de-intercalation direction, resulting in films with different crystallographic orientations[155]. This further expands our ability to prepare single-crystalline nickelates with distinct lattice symmetries and coordination configurations, which can lead to a wide range of enriched properties.

***Magnetism.*** Magnetic 2D materials can also be prepared by intercalation of transition metals through bonding and doping effects. The covalent bonds formed between the intercalants and the host lattice can alter the properties of the *d* orbitals of the transition metals through hybridization and charge redistribution, thus affecting the magnetic properties. For example, in tantalum-intercalated $TaS_2$ bilayers, when each intercalated tantalum atom is bonded with six sulfur atoms to form an octahedral superstructure, additional spin-split bands across the Fermi level can be observed[71] (FIG. 4e) and a magnetic ground state develops. Similar phenomena were also discovered in other compounds intercalated with transition metals[65,156–158].

The tunability of 2D magnetism via intercalation has also drawn considerable attention. One example is the transition from a ferromagnetic semiconducting to a ferromagnetic metallic phase with an enhanced Curie temperature in $Cr_2Ge_2Te_6$ via organic molecule intercalation, which can be attributed to the change of magnetic coupling from a weak super-exchange interaction to a strong double-exchange interaction upon doping[54]. In addition, interlayer coupling plays an essential role in 2D magnetism. Calculations show that lithium-ion intercalation in bilayer $Fe_3GeTe_2$ provides hopping carriers between the two interfacial tellurium sublayers, leading to an enhancement of the interlayer ferromagnetic coupling at a relatively low intercalation level[159]. Recently, the interlayer magnetic coupling of $Fe_3GeTe_2$ was shown to be dramatically enhanced through proton intercalation, as evidenced by exchange bias in transport measurements[160]. However, an experimental approach to quantify the strength of intercalation-induced interlayer exchange coupling is yet to be fully developed.

***Structural phase transitions.*** In van der Waals materials, although the intercalation method is viewed as a mild reaction that does not greatly affect the host lattice, lattice variations and structural transitions resulting from the presence of guest species can be highly relevant in some circumstances. In-plane lattice variations are usually driven by disorder, substitutions and/or structural phase transitions. One intriguing phase transition is the transition from the semiconducting 2H phase to the metallic 1T phase in lithium-intercalated $MoS_2$ (REFS.[76,161–163]). The driving mechanism, attributed to the drastic increase in the electronic energy of the semiconducting host because of charge transfer from the lithium intercalant, can also be applicable to phase transitions of other group VIB TMDs upon lithium intercalation. Metastable phases such as the 1T′ phase have also been observed in lithium-intercalated $MoS_2$ (REF.[164]). Recently, electrochemical intercalation of exceptionally few lithium ions into $WTe_2$ induced large anisotropic in-plane strain, which was linked to the formation of a new phase with an exotic atomic and crystallographic arrangement[165]. Substitution in the host 2D material can contribute to structural transitions as well. For example, copper is easy to intercalate and undergo substitution in $Bi_2Se_3$ (REFS.[132,166]).

In addition to the understanding of the intercalation process and the resulting compounds, the discovery of new properties has spurred extensive research efforts, leading to new device designs. For example, the catalytic performance of TMDs is modulated upon alkali metal intercalation[89,167] and metallic $MoS_2$ in the 1T phase has been used to fabricate low-resistance contacts for 2H-$MoS_2$ transistors[168]. Additionally, a thermal transistor has been fabricated through intercalation and de-intercalation of lithium in $MoS_2$, where the enhanced phonon scattering, *c*-axis strain and stacking disorder resulted in a thermal ON/OFF ratio of ~10 (REF.[169]).

The *c*-axis lattice expansion is another direct consequence of intercalation, especially for the intercalation of large organic molecules. The weak interlayer van der Waals interaction allows the layers to separate to accommodate the intercalated organic molecules[170] in response to an external driving force, such as concentration or voltage gradients, minimizing the system energy. The separation of each layer can result in a 3D to 2D electronic transition. As an example, pyridine intercalated into $TaS_2$ increased the interlayer distance from 6 Å to 12 Å, leading to the emergence of 2D superconducting properties in 3D bulk $TaS_2$. These new types of

intercalation compounds were denoted as organometallic crystals[72,170]. More recently, semiconducting 2D materials have been intercalated with long-chain alkyl ammonium bromide to create monolayer atomic crystal molecular superlattices, leading to single-layer properties in vertically integrated (quasi-)bulk 2D materials that are sensitive to ambient conditions, such as black phosphorus[171,172] (FIG. 4f). Interlayer expansion also induces strain in the materials, which can be used to manipulate the mechanical behaviour in actuator applications or to control the electronic band structure for catalysis[173,174].

***Phonon and photon transport.*** Considerable progress has also been achieved in the study of phonon and photon transport in guest species-modulated 2D materials, leading to breakthroughs in thermoelectric, photoelectric and optoelectronic materials. For example, the cross-plane thermal conductivity can be reduced by one order of magnitude through the intercalation of lithium, which is attributed to phonon scattering by intercalants and intercalation-induced structural changes and disorder[169]. In addition, n-type flexible thermoelectric materials with a high figure of merit were synthesized through the electrochemical intercalation of organic molecules into $TiS_2$ (REF.[175]). As for photon transport measurements, numerous studies have also demonstrated the control of optical properties by intercalation[176,177]. For example, copper intercalation in $Bi_2E_3$, where E is either selenium or tellurium, leads to a significant enhancement of light transmission owing to both a reduction in absorption after the intercalation and to the nanophotonic effect of zero-wave anti-reflection, attributable to the ultra-small thickness of the nanoplates[178]. Another important example is $SnS_2$, where the colours of the crystals change dramatically upon different atom intercalation, and significantly different relative reflectance can be observed, indicating a tuning of the electronic band structure and optical properties[179] (FIG. 4g).

## Perspectives

In recent years, research on guest-species modulation of 2D materials has witnessed tremendous development. The expanding toolbox of accessible modulation techniques and 2D systems creates a new dimension for materials design and device applications.

Many potential device applications based on guest-species modulation have been investigated. In particular, the strong tuning of the carrier density enabled the early development of nanoscale transistors and optoelectronic devices[180,181]. In recent years, guest-species tuning of additional materials properties enabled the design of new transistor architectures. For instance, ionic[182], catalytic[183] and thermal transistors[169] have been fabricated to control the ON/OFF state using different parameters and functionalities, such as ionic diffusivity, catalytic performance and thermal conductivity, respectively. Despite the great potential for applications, more work is needed to expand the library of guest species and address the challenges in mass production, integration and durability related to the practical use of these devices.

So far, the gating method has been mainly used to achieve a high carrier density in 2D materials. Therefore, the choice of the gating guest species, or their combinations, is commonly limited to monovalent cations or ions without degrees of freedom in charge and chemical valence. The introduction of 3*d* orbital electrons in ionic media may result in novel phenomena and quantum phases: for instance, by introducing paramagnetic ions ($FeCl_4^-$) with unpaired 3*d* orbitals in platinum thin films, reversible electrical switching of ferromagnetic states was obtained[184]. Even though this technique presents fertile ground for the exploration of 2D magnetism, the utilization of ionic gating with 3*d* metal ions has not been widely adopted. Benefitting from battery research, alkali metal intercalation has been studied for decades, and well-controlled intercalation methods have been developed successfully. However, the intercalation of multivalent 3*d* metal ions with various orbitals and electron clouds still needs more investigation. Current multivalent 3*d* metal intercalation strategies are mainly based on solid-state reactions at high temperatures with a fixed concentration of intercalants. A dynamically tunable approach to control the intercalation of multivalent 3*d* metals is urgently needed for the development of novel low-dimensional materials.

In contrast with the cation intercalation approaches discussed above, research on anion intercalation is still not fully developed. Oxidative anion insertion processes offer many opportunities for the rational design and selective synthesis of a broad range of novel metastable materials. A good example is the soft fluorination chemistry involving both anion insertion[185] and exchange with large oxidizing potential[186] at low temperatures, which has been used to tune the electronic behaviour of copper oxides to induce high-temperature superconductivity[187–189]. The discovery of new reagents and related topochemistry, which results in a larger variety of possible topotactic transformations, enables the preparation of metastable complex phases on demand.

In addition to the increase of possible guest species available for modulation, host 2D materials are also facing new opportunities. Artificial structures created by stacking different layers provide a unique platform for intercalation reactions, yet the intercalation chemistry and physics of the 2D artificial structure remain unexplored. A higher capacity and larger negative intercalation potential have been measured by intercalating lithium into a series of van der Waals heterostructures based on stacked hexagonal boron nitride, graphene and $MoX_2$, where X can be sulfur or selenium[190]. Key characteristics of intercalation reactions are determined by the crystallographic and electronic structures of the host material. Thus, by stacking layers from different materials together, the properties of the resulting material can be engineered. Along this path, twisted 2D materials with Moiré patterns stand out as interesting candidates for guest-species insertion, as theoretical studies have indicated localized energy-favourable positions for introduced guest species in the Moiré lattice. This insertion may then produce unique band structures and properties[191–193]. Furthermore, the roll-up of 2D materials could extend guest-species modulation from 2D to 1D systems[194] and provide more opportunities to study the interactions of guest species beyond 2D materials[195].

Furthermore, there are intriguing lattice orderings emerging concurrently with ionic rearrangements in topochemical intercalations, such as spontaneously formed oxygen vacancy-ordered structures[113,196], in which the ordering of oxygen vacancies and of cationic sites along certain preferred directions can occur simultaneously. This motivates the idea of dual-intercalation procedures involving both cationic insertion and anionic de-intercalation, or even sequential topochemical synthetic reactions. In addition, the different coordination preference of the transition metal ions plays a decisive role in forming the ionic framework in the lattice. Exemplified by infinite-layer nickelates, the guest-species modulation of 2D thin films provides opportunities for the stabilization of unconventional complex materials, where the crystal-field environment and lattice symmetry can be further perturbed and controlled by the choice of substrate and the consequentially induced epitaxial strain, particularly at hetero-interfaces.

In addition to new modulation methods, further developments are needed for scalable integration at the system level. Large-scale modulation methods are essential for mass production. Although recent reports have shown that some intercalation methods have the potential for scale-up[71,197], some tuning methods still require more efforts to achieve a scalable production. Another important aspect is the liquid or gel nature of most ionic gating media, which complicates the integration with modern on-chip semiconductor technologies, partly due to difficulties in controlling the size and shape of the ionic liquid or gel[198]. As a result, widely implemented ionic gating techniques are largely limited to single devices, and broader applications in integrated circuits are still relatively far off. In this regard, solid-state ionic gating materials[21,39,41] are particularly exciting due to their likely compatibility with lithography and deposition processes, going beyond single-device applications. Last but not least, guest-species modulation methods may have fundamental issues with stability and durability, particularly in harsh environments[162]. Therefore, developing smart strategies for the assembly, encapsulation and packaging of guest species-modulated devices is crucial for future applications.

Published online 31 August 2022


1. Ahn, C. H. et al. Electrostatic modification of novel materials. *Rev. Mod. Phys.* **78**, 1185–1212 (2006).
2. Norris, D. J., Efros, A. L. & Erwin, S. C. Doped nanocrystals. *Science* **319**, 1776–1779 (2008).
3. Chen, Y. et al. Phase engineering of nanomaterials. *Nat. Rev. Chem.* **4**, 243–256 (2020).
4. Ning, C. Z., Dou, L. T. & Yang, P. D. Bandgap engineering in semiconductor alloy nanomaterials with widely tunable compositions. *Nat. Rev. Mater.* **2**, 17070 (2017).
5. Tsutsui, G., Mochizuki, S., Loubet, N., Bedell, S. W. & Sadana, D. K. Strain engineering in functional materials. *AIP Adv.* **9**, 030701 (2019).
6. Novoselov, K. S., Mishchenko, A., Carvalho, A. & Neto, A. H. C. 2D materials and van der Waals heterostructures. *Science* **353**, aac9439 (2016).
7. Manzeli, S., Ovchinnikov, D., Pasquier, D., Yazyev, O. V. & Kis, A. 2D transition metal dichalcogenides. *Nat. Rev. Mater.* **2**, 17033 (2017).
8. Novoselov, K. S. et al. Two-dimensional atomic crystals. *Proc. Natl Acad. Sci. USA* **102**, 10451–10453 (2005).
9. Dresselhaus, M. S. *Intercalation in Layered Materials* Vol. 148 (Springer, 1986).
**This comprehensive survey of intercalation of bulk layered crystals emphasizes the physics of intercalation and the complementarity of intercalated materials and deliberately structured superlattices formed by various techniques**.
10. Liu, X. L. & Hersam, M. C. 2D materials for quantum information science. *Nat. Rev. Mater.* **4**, 669–684 (2019).
11. Iannaccone, G., Bonaccorso, F., Colombo, L. & Fiori, G. Quantum engineering of transistors based on 2D materials heterostructures. *Nat. Nanotechnol.* **13**, 183–191 (2018).
12. Pomerantseva, E. & Gogotsi, Y. Two-dimensional heterostructures for energy storage. *Nat. Energy* **2**, 17089 (2017).
13. Tokura, Y. & Nagaosa, N. Orbital physics in transition-metal oxides. *Science* **288**, 462–468 (2000).
14. Dagotto, E. Complexity in strongly correlated electronic systems. *Science* **309**, 257–262 (2005).
15. Ramesh, R. & Spaldin, N. A. Multiferroics: progress and prospects in thin films. *Nat. Mater.* **6**, 21–29 (2007).
16. Keimer, B., Kivelson, S. A., Norman, M. R., Uchida, S. & Zaanen, J. From quantum matter to high-temperature superconductivity in copper oxides. *Nature* **518**, 179–186 (2015).
17. Imada, M., Fujimori, A. & Tokura, Y. Metal-insulator transitions. *Rev. Mod. Phys.* **70**, 1039–1263 (1998).
18. Yuan, H. T. et al. High-density carrier accumulation in ZnO field-effect transistors gated by electric double layers of ionic liquids. *Adv. Funct. Mater.* **19**, 1046–1053 (2009).
19. Largeot, C. et al. Relation between the ion size and pore size for an electric double-layer capacitor. *J. Am. Chem. Soc.* **130**, 2730 (2008).
20. Zhang, Y., Ye, J., Matsuhashi, Y. & Iwasa, Y. Ambipolar $MoS_2$ thin flake transistors. *Nano Lett.* **12**, 1136–1140 (2012).
**This study is one of the early demonstrations of 2D materials transistors with ionic liquid gating**.
21. Wu, C. L. et al. Gate-induced metal-insulator transition in $MoS_2$ by solid superionic conductor $LaF_3$. *Nano Lett.* **18**, 2387–2392 (2018).
22. Fujimoto, T. & Awaga, K. Electric-double-layer field-effect transistors with ionic liquids. *Phys. Chem. Chem. Phys.* **15**, 8983–9006 (2013).
23. Armand, M., Endres, F., MacFarlane, D. R., Ohno, H. & Scrosati, B. Ionic-liquid materials for the electrochemical challenges of the future. *Nat. Mater.* **8**, 621–629 (2009).
24. Yuan, H. T. et al. Liquid-gated ambipolar transport in ultrathin films of a topological insulator $Bi_2Te_3$. *Nano Lett.* **11**, 2601–2605 (2011).
25. Allain, A. & Kis, A. Electron and hole mobilities in single-layer $WSe_2$. *ACS Nano* **8**, 7180–7185 (2014).
26. Saito, Y. & Iwasa, Y. Ambipolar insulator-to-metal transition in black phosphorus by ionic-liquid gating. *ACS Nano* **9**, 3192–3198 (2015).
27. Ye, J. T. et al. Superconducting dome in a gate-tuned band insulator. *Science* **338**, 1193–1196 (2012).
28. Ye, J. T. et al. Liquid-gated interface superconductivity on an atomically flat film. *Nat. Mater.* **9**, 125–128 (2010).
29. Ueno, K. et al. Discovery of superconductivity in $KTaO_3$ by electrostatic carrier doping. *Nat. Nanotechnol.* **6**, 408–412 (2011).
30. Yu, Y. J. et al. Gate-tunable phase transitions in thin flakes of 1T-$TaS_2$. *Nat. Nanotechnol.* **10**, 270–276 (2015).
31. Ozel, T., Gaur, A., Rogers, J. A. & Shim, M. Polymer electrolyte gating of carbon nanotube network transistors. *Nano Lett.* **5**, 905–911 (2005).
32. Lin, M. W. et al. Mobility enhancement and highly efficient gating of monolayer $MoS_2$ transistors with polymer electrolyte. *J. Phys. D.* **45**, 345102 (2012).
33. Pu, J. et al. Highly flexible $MoS_2$ thin-film transistors with ion gel dielectrics. *Nano Lett.* **12**, 4013–4017 (2012).
34. Pu, J. et al. Fabrication of stretchable $MoS_2$ thin-film transistors using elastic ion-gel gate dielectrics. *Appl. Phys. Lett.* **103**, 023505 (2013).
35. McCann, D. M., Misek, M., Kamenev, K. V. & Huxley, A. D. Pressure-temperature phase diagram of ionic liquid dielectric DEME-TFSI. *Phys. Procedia* **75**, 252–258 (2015).
36. Lu, A. X., Sun, J., Jiang, J. & Wan, Q. Microporous $SiO_2$ with huge electric-double-layer capacitance for low-voltage indium tin oxide thin-film transistors. *Appl. Phys. Lett.* **95**, 222905 (2009).
37. Liu, H. X., Sun, J., Tang, Q. X. & Wan, Q. Ultra low-voltage electric double-layer $SnO_2$ nanowire transistors gated by microporous $SiO_2$-based solid electrolyte. *J. Phys. Chem. C.* **114**, 12316–12319 (2010).
38. Chao, J. Y., Zhu, L. Q., Xiao, H. & Yuan, Z. G. Protonic/electronic hybrid oxide transistor gated by chitosan and its full-swing low voltage inverter applications. *J. Appl. Phys.* **118**, 235301 (2015).
39. Zhao, J. L. et al. Lithium-ion-based solid electrolyte tuning of the carrier density in graphene. *Sci. Rep.* **6**, 34816 (2016).
40. Alam, M. H. et al. Lithium-ion electrolytic substrates for sub-1V high-performance transition metal dichalcogenide transistors and amplifiers. *Nat. Commun.* **11**, 3203 (2020).
41. Zhao, J. L. et al. Application of sodium-ion-based solid electrolyte in electrostatic tuning of carrier density in graphene. *Sci. Rep.* **7**, 3168 (2017).
42. Zhang, S., Wang, J., Lu, X. & Zhou, Q. *Structures and Interactions of Ionic Liquids* Vol. 151 (Springer, 2013).
43. Radisavljevic, B., Radenovic, A., Brivio, J., Giacometti, V. & Kis, A. Single-layer $MoS_2$ transistors. *Nat. Nanotechnol.* **6**, 147–150 (2011).
44. Palumbo, F. et al. A review on dielectric breakdown in thin dielectrics: silicon dioxide, high-*k*, and layered dielectrics. *Adv. Funct. Mater.* **30**, 1900657 (2020).
45. Desai, S. B. et al. $MoS_2$ transistors with 1-nanometer gate lengths. *Science* **354**, 99–102 (2016).
46. Veyrat, L. et al. Helical quantum Hall phase in graphene on $SrTiO_3$. *Science* **367**, 781–786 (2020).
47. Saito, Y., Nojima, T. & Iwasa, Y. Highly crystalline 2D superconductors. *Nat. Rev. Mater.* **2**, 16094 (2017).
**This review focuses on the physical properties of highly crystalline 2D superconductors, and discusses the electric field-controlled superconductivity by EDLTs**.
48. Zheliuk, O. et al. Josephson coupled Ising pairing induced in suspended $MoS_2$ bilayers by double-side ionic gating. *Nat. Nanotechnol.* **14**, 1123–1128 (2019).
49. Nakagawa, Y. et al. Gate-controlled BCS–BEC crossover in a two-dimensional superconductor. *Science* **372**, 190–195 (2021).
50. Li, L. J. et al. Controlling many-body states by the electric-field effect in a two-dimensional material. *Nature* **529**, 185–189 (2016).
51. Shiogai, J., Ito, Y., Mitsuhashi, T., Nojima, T. & Tsukazaki, A. Electric-field-induced superconductivity in electrochemically etched ultrathin FeSe films on $SrTiO_3$ and MgO. *Nat. Phys.* **12**, 42–46 (2016).
52. Deng, Y. et al. Gate-tunable room-temperature ferromagnetism in two-dimensional $Fe_3GeTe_2$. *Nature* **563**, 94–99 (2018).
53. Wang, Z. et al. Electric-field control of magnetism in a few-layered van der Waals ferromagnetic semiconductor. *Nat. Nanotechnol.* **13**, 554–559 (2018).

54. Verzhbitskiy, I. A. et al. Controlling the magnetic anisotropy in $Cr_2Ge_2Te_6$ by electrostatic gating. *Nat. Electron.* **3**, 460–465 (2020).
55. Li, Y., Duerloo, K. A. N., Wauson, K. & Reed, E. J. Structural semiconductor-to-semimetal phase transition in two-dimensional materials induced by electrostatic gating. *Nat. Commun.* **7**, 10671 (2016).
56. Wang, Y. et al. Structural phase transition in monolayer $MoTe_2$ driven by electrostatic doping. *Nature* **550**, 487–491 (2017).
57. Zakhidov, D., Rehn, D. A., Reed, E. J. & Salleo, A. Reversible electrochemical phase change in monolayer to bulk-like $MoTe_2$ by ionic liquid gating. *ACS Nano* **14**, 2894–2903 (2020).
58. Datta, I. et al. Low-loss composite photonic platform based on 2D semiconductor monolayers. *Nat. Photonics* **14**, 256 (2020).
59. Yuan, H. T. et al. Electrostatic and electrochemical nature of liquid-gated electric-double-layer transistors based on oxide semiconductors. *J. Am. Chem. Soc.* **132**, 18402–18407 (2010).
60. Lu, J. M. et al. Evidence for two-dimensional ising superconductivity in gated $MoS_2$. *Science* **350**, 1353–1357 (2015).
61. Lee, S. J. et al. Programmable devices based on reversible solid-state doping of two-dimensional semiconductors with superionic silver iodide. *Nat. Electron.* **3**, 630–637 (2020).
62. Koski, K. J. et al. Chemical intercalation of zerovalent metals into 2D layered $Bi_2Se_3$ nanoribbons. *J. Am. Chem. Soc.* **134**, 13773–13779 (2012).
63. Wang, M. J. et al. Chemical intercalation of heavy metal, semimetal, and semiconductor atoms into 2D layered chalcogenides. *2D Mater.* **5**, 045005 (2018).
64. Mckelvey, M., Sharma, R., Ong, E., Burr, G. & Glaunsinger, W. Dynamic atomic-level observation of staging phenomena in silver and mercury intercalates of titanium disulfide. *Chem. Mater.* **3**, 783–786 (1991).
65. Parkin, S. & Friend, R. 3*d* transition-metal intercalates of the niobium and tantalum dichalcogenides. I. Magnetic properties. *Philos. Mag. B* **41**, 65–93 (1980).
66. Parkin, S. & Friend, R. 3*d* transition-metal intercalates of the niobium and tantalum dichalcogenides. II. Transp. properties. *Philos. Mag. B* **41**, 95–112 (1980).
67. Vickery, R. C. & Campbell, N. L. Rare earth graphite intercalates. *J. Am. Chem. Soc.* **79**, 5897–5899 (1957).
68. Zhang, L. F. et al. 2D atomic crystal molecular superlattices by soft plasma intercalation. *Nat. Commun.* **11**, 5960 (2020).
69. Grenier, J. C. et al. Electrochemical oxygen intercalation into oxide networks. *J. Solid State Chem.* **96**, 20–30 (1992).
70. Hartwigsen, C., Witschel, W. & Spohr, E. Charge density and charge transfer in stage-1 alkali-graphite intercalation compounds. *Phys. Rev. B* **55**, 4953–4959 (1997).
71. Zhao, X. X. et al. Engineering covalently bonded 2D layered materials by self-intercalation. *Nature* **581**, 171–177 (2020).
72. Gamble, F. R., Osiecki, J. H. & Disalvo, F. J. Some superconducting intercalation complexes of $TaS_2$ and substituted pyridines. *J. Chem. Phys.* **55**, 3525 (1971).
73. Rao, G. V. S., Shafer, M. W. & Tsang, J. C. Intercalation compounds of metal-hydroxides with group V layered dichalcogenides. *J. Phys. Chem.* **79**, 553–557 (1975).
74. Stumpp, E. The intercalation of metal chlorides and bromides into graphite. *Mater. Sci. Eng.* **31**, 53–59 (1977).
75. Yeh, I. C. & Hummer, G. System-size dependence of diffusion coefficients and viscosities from molecular dynamics simulations with periodic boundary conditions. *J. Phys. Chem. B* **108**, 15873–15879 (2004).
76. Zhang, J. S. et al. Reversible and selective ion intercalation through the top surface of few-layer $MoS_2$. *Nat. Commun.* **9**, 5289 (2018).
77. Koski, K. J. et al. High-density chemical intercalation of zero-valent copper into $Bi_2Se_3$ nanoribbons. *J. Am. Chem. Soc.* **134**, 7584–7587 (2012).
78. Van der Ven, A., Bhattacharya, J. & Belak, A. A. Understanding Li diffusion in Li-intercalation compounds. *Acc. Chem. Res.* **46**, 1216–1225 (2013).
79. Friend, R. H. & Yoffe, A. D. Electronic-properties of intercalation complexes of the transition-metal dichalcogenides. *Adv. Phys.* **36**, 1–94 (1987).
80. Rao, C. N. R., Raveau, B., *Colossal Magnetoresistance, Charge Ordering and Related Properties of Manganese Oxides* (World Scientific, 1998).
81. Winter, M., Besenhard, J. O., Spahr, M. E. & Novak, P. Insertion electrode materials for rechargeable lithium batteries. *Adv. Mater.* **10**, 725–763 (1998).
82. Mulhern, P. J. Lithium intercalation in crystalline $Li_xMoS_2$. *Can. J. Phys.* **67**, 1049–1052 (1989).
83. Sole, C., Drewett, N. E. & Hardwick, L. J. In situ Raman study of lithium-ion intercalation into microcrystalline graphite. *Faraday Discuss.* **172**, 223–237 (2014).
84. Grenier, J. C., Pouchard, M. & Wattiaux, A. Electrochemical synthesis: oxygen intercalation. *Curr. Opin. Solid State Mater. Sci.* **1**, 233–240 (1996).
85. Julien, C. M. Lithium intercalated compounds — charge transfer and related properties. *Mat. Sci. Eng. R.* **40**, 47–102 (2003).
86. Reimers, J. N. & Dahn, J. Electrochemical and in situ X-ray diffraction studies of lithium intercalation in $Li_xCoO_2$. *J. Electrochem. Soc.* **139**, 2091 (1992).
87. Chen, Z. H., Lu, Z. H. & Dahn, J. R. Staging phase transitions in $Li_xCoO_2$. *J. Electrochem. Soc.* **149**, A1604 (2002).
88. Daheron, L. et al. Electron transfer mechanisms upon lithium deintercalation from $LiCoO_2$ to $CoO_2$ investigated by XPS. *Chem. Mater.* **20**, 583–590 (2008).
89. Lu, Z. Y., Jiang, K., Chen, G. X., Wang, H. T. & Cui, Y. Lithium electrochemical tuning for electrocatalysis. *Adv. Mater.* **30**, 1800978 (2018).
90. Bae, J. et al. Kinetic 2D crystals via topochemical approach. *Adv. Mater.* **30**, 2006043 (2021).
91. Ranmohotti, K. G. S., Josepha, E., Choi, J., Zhang, J. X. & Wiley, J. B. Topochemical manipulation of perovskites: low-temperature reaction strategies for directing structure and properties. *Adv. Mater.* **23**, 442–460 (2011).
92. Dines, M. B. Lithium intercalation via *n*-Butyllithium of the layered transition metal dichalcogenides. *Mater. Res. Bull.* **10**, 287–291 (1975).
93. Liu, R. et al. Intercalating copper into layered $TaS_2$ van der Waals gaps. *Rsc Adv.* **7**, 46699–46703 (2017).
94. Motter, J. P., Koski, K. J. & Cui, Y. General strategy for zero-valent intercalation into two-dimensional layered nanomaterials. *Chem. Mater.* **26**, 2313–2317 (2014).
95. Zhong, Q., Dahn, J. R. & Colbow, K. Lithium intercalation into $WO_3$ and the phase-diagram of $Li_xWO_3$. *Phys. Rev. B* **46**, 2554–2560 (1992).
96. Dahn, J. R. & Mckinnon, W. R. Structure and electrochemistry of $Li_xMoO_2$. *Solid State Ion.* **23**, 1–7 (1987).
97. Jiao, F. & Bruce, P. G. Mesoporous crystalline β-$MnO_2$ — a reversible positive electrode for rechargeable lithium batteries. *Adv. Mater.* **19**, 657–660 (2007).
98. Kim, C. et al. Direct observation of reversible magnesium ion intercalation into a spinel oxide host. *Adv. Mater.* **27**, 3377–3384 (2015).
99. Moshopoulou, E. G. Superconductivity in the spinel compound $LiTi_2O_4$. *J. Am. Ceram. Soc.* **82**, 3317–3320 (1999).
100. Yoshimatsu, K., Niwa, M., Mashiko, H., Oshima, T. & Ohtomo, A. Reversible superconductor-insulator transition in $LiTi_2O_4$ induced by Li-ion electrochemical reaction. *Sci. Rep.* **5**, 16325 (2015).
101. Golub, A. S., Protzenko, G. A., Yanovskaya, I. M., Lependina, O. L. & Novikov, Y. N. New intercalation compounds of molybdenum-disulfide with transition-metals, $A_x(H2O)_yMoS_2$ (A = Fe, Co, Ni, Y, La, Er, Th). *Mendeleev Commun.* **3**, 199–200 (1993).
102. Chen, Z. X. et al. Interface confined hydrogen evolution reaction in zero valent metal nanoparticles-intercalated molybdenum disulfide. *Nat. Commun.* **8**, 14548 (2017).
103. Luo, Y. T. et al. Two-dimensional $MoS_2$ confined $Co(OH)_2$ electrocatalysts for hydrogen evolution in alkaline electrolytes. *ACS Nano* **12**, 4565–4573 (2018).
104. Zou, Y. C. et al. Ion exchange in atomically thin clays and micas. *Nat. Mater.* **20**, 1677–1682 (2021).
105. Poeppelmeier, K. R., Leonowicz, M. E. & Longo, J. M. $CaMnO_{2.5}$ and $Ca_2MnO_{3.5}$ — new oxygen-defect perovskite-type oxides. *J. Solid State Chem.* **44**, 89–98 (1982).
106. Briatico, J. et al. Double-exchange interaction in electron-doped $CaMnO_{3-\delta}$ perovskites. *Phys. Rev. B* **53**, 14020–14023 (1996).
107. Zhang, J. J. et al. Large orbital polarization in a metallic square-planar nickelate. *Nat. Phys.* **13**, 864–869 (2017).
108. Hansteen, O. H., Fjellvag, H. & Hauback, B. C. Crystal structure and magnetic properties of $La_2Co_2O_5$. *J. Solid State Chem.* **141**, 411–417 (1998).
109. Hayward, M. A., Green, M. A., Rosseinsky, M. J. & Sloan, J. Sodium hydride as a powerful reducing agent for topotactic oxide deintercalation: synthesis and characterization of the nickel(I) oxide $LaNiO_2$. *J. Am. Chem. Soc.* **121**, 8843–8854 (1999).
110. Hayward, M. A. & Rosseinsky, M. J. Synthesis of the infinite layer Ni(I) phase $NdNiO_{2+x}$ by low temperature reduction of $NdNiO_3$ with sodium hydride. *Solid State Sci.* **5**, 839–850 (2003).
111. Kawai, M. et al. Reversible changes of epitaxial thin films from perovskite $LaNiO_3$ to infinite-layer structure $LaNiO_2$. *Appl. Phys. Lett.* **94**, 082102 (2009).
112. Tsujimoto, Y. et al. Infinite-layer iron oxide with a square-planar coordination. *Nature* **450**, 1062–1065 (2007).
113. Hayward, M. A. Topochemical reactions of layered transition-metal oxides. *Semicond. Sci. Tech.* **29**, 064010 (2014).
114. Kaneko, D., Yamagishi, K., Tsukada, A., Manabe, T. & Naito, M. Synthesis of infinite-layer $LaNiO_2$ films by metal organic decomposition. *Phys. C.* **469**, 936–939 (2009).
115. Hadermann, J., Abakumov, A. M., Adkin, J. J. & Hayward, M. A. Topotactic reduction as a route to new close-packed anion deficient perovskites: structure and magnetism of 4H-$BaMnO_{2+x}$. *J. Am. Chem. Soc.* **131**, 10598–10604 (2009).
116. Ikeda, A., Manabe, T. & Naito, M. Comparison of reduction agents in the synthesis of infinite-layer $LaNiO_2$ films. *Phys. C.* **506**, 83–86 (2014).
117. Shimakawa, Y. et al. Topotactic changes in thin films of brownmillerite $SrFeO_{2.5}$ grown on $SrTiO_3$ substrates to infinite-layer structure $SrFeO_2$. *Cryst. Growth Des.* **10**, 4713–4715 (2010).
118. Kawakami, T. et al. Spin transition in a four-coordinate iron oxide. *Nat. Chem.* **1**, 371–376 (2009).
119. Zubko, P., Gariglio, S., Gabay, M., Ghosez, P. & Triscone, J. M. Interface physics in complex oxide heterostructures. *Annu. Rev. Condens. Matter Phys.* **2**, 141–165 (2011).
120. Hwang, H. Y. et al. Emergent phenomena at oxide interfaces. *Nat. Mater.* **11**, 103–113 (2012).
121. Poltavets, V. V. et al. $La_3Ni_2O_6$: a new double T′-type nickelate with infinite $Ni^{1+/2+}O_2$ layers. *J. Am. Chem. Soc.* **128**, 9050–9051 (2006).
122. Poltavets, V. V. et al. Bulk magnetic order in a two-dimensional $Ni^{1+}/Ni^{2+}$ ($d(9)/d(8)$) nickelate, isoelectronic with superconducting cuprates. *Phys. Rev. Lett.* **104**, 206403 (2010).
123. Lacorre, P. Passage from T-type to T′-type arrangement by reducing $R_4Ni_3O_{10}$ to $R_4Ni_3O_8$ (R = La, Pr, Nd). *J. Solid State Chem.* **97**, 495–500 (1992).
124. Zhang, J. J. et al. Stacked charge stripes in the quasi-2D trilayer nickelate $La_4Ni_3O_8$. *Proc. Natl Acad. Sci. USA* **113**, 8945–8950 (2016).
125. Zhang, J. J. et al. Spin stripe order in a square planar trilayer nickelate. *Phys. Rev. Lett.* **122**, 247201 (2019).
126. Norman, M. R. Materials design for new superconductors. *Rep. Prog. Phys.* **79**, 074502 (2016).
127. Li, D. et al. Superconductivity in an infinite-layer nickelate. *Nature* **572**, 624–627 (2019). **This study demonstrates superconductivity in an infinite-layer nickelate structure formed by soft-chemistry de-intercalation**.
128. Norman, M. R. Entering the nickel age of superconductivity. *Physics* **13**, 85 (2020).
129. Jung, N. et al. Charge transfer chemical doping of few layer graphenes: charge distribution and band gap formation. *Nano Lett.* **9**, 4133–4137 (2009).
130. Ahmad, S., Miro, P., Audiffred, M. & Heine, T. Tuning the electronic structure of graphene through alkali metal and halogen atom intercalation. *Solid State Commun.* **272**, 22–27 (2018).
131. Hagenmuller, P. Intercalation chemistry and chemical bonding. *J. Phys. Chem. Solids* **59**, 503–506 (1998).
132. Shetty, P. P. et al. In situ dynamics during heating of copper-intercalated bismuth telluride. *Matter* **3**, 1246–1262 (2020).
133. Viciu, L. et al. Crystal structure and elementary properties of $Na_xCoO_2$ ($x$ = 0.32, 0.51, 0.6, 0.75, and 0.92) in the three-layer $NaCoO_2$ family. *Phys. Rev. B* **73**, 174104 (2006).
134. Fouassier, C., Matejka, G., Reau, J.-M. & Hagenmuller, P. Sur de nouveaux bronzes oxygénés de formule $Na_xCoO_2$ ($\chi$1). Le système cobalt–oxygène–sodium. *J. Solid State Chem.* **6**, 532–537 (1973).
135. Huang, Q. et al. Coupling between electronic and structural degrees of freedom in the triangular lattice conductor $Na_xCoO_2$. *Phys. Rev. B* **70**, 184110 (2004).
136. Delmas, C., Braconnier, J. J., Fouassier, C. & Hagenmuller, P. Electrochemical Intercalation of sodium in $Na_xCoO_2$ bronzes. *Solid State Ion.* **3–4**, 165–169 (1981).

137. Motohashi, T. et al. Electronic phase diagram of the layered cobalt oxide system $Li_xCoO_2$ ($0.0 \leq x \leq 1.0$). *Phys. Rev. B* **80**, 165114 (2009).
138. Foo, M. L. et al. Charge ordering, commensurability, and metallicity in the phase diagram of the layered $Na_xCoO_2$. *Phys. Rev. Lett.* **92**, 247001 (2004).
139. Ong, N. P. & Cava, R. J. Electronic frustration on a triangular lattice. *Science* **305**, 52–53 (2004).
140. Takada, K. et al. Superconductivity in two-dimensional $CoO_2$ layers. *Nature* **422**, 53–55 (2003).
141. Schaak, R. E., Klimczuk, T., Foo, M. L. & Cava, R. J. Superconductivity phase diagram of $Na_xCoO_2 \times 1.3H_2O$. *Nature* **424**, 527–529 (2003).
142. Milne, C. J. et al. Revised superconducting phase diagram of hole-doped $Na_x(H_3O)_zCoO_2 \cdot yH_2O$. *Phys. Rev. Lett.* **93**, 247007 (2004).
143. Sakurai, H., Takada, K., Sasaki, T. & Takayama-Muromachi, E. Phase diagram of superconducting $Na_xCoO_2 \cdot yH_2O$. *J. Phys. Soc. Jpn.* **74**, 2909–2912 (2005).
144. Sakurai, H., Takada, K., Sasaki, T. & Takayama-Muromachi, E. Superconducting phase diagram of $Na_xCoO_2 \cdot yH_2O$. *Phys. C.* **445**, 31–34 (2006).
145. Sakurai, H. et al. Valence and Na content dependences of superconductivity in $Na_xCoO_2 \cdot yH_2O$. *Phys. Rev. B* **74**, 092502 (2006).
146. Terasaki, I., Sasago, Y. & Uchinokura, K. Large thermoelectric power in $NaCo_2O_4$ single crystals. *Phys. Rev. B* **56**, 12685–12687 (1997).
147. Ray, R., Ghoshray, A., Ghoshray, K. & Nakamura, S. Co-59 NMR studies of metallic $NaCo_2O_4$. *Phys. Rev. B* **59**, 9454–9461 (1999).
148. Wang, Y. Y., Rogado, N. S., Cava, R. J. & Ong, N. P. Spin entropy as the likely source of enhanced thermopower in $Na_xCo_2O_4$. *Nature* **423**, 425–428 (2003).
149. Crespin, M., Levitz, P. & Gatineau, L. Reduced forms of $LaNiO_3$ perovskite. 1. Evidence for new phases — $La_2Ni_2O_5$ and $LaNiO_2$. *J. Chem. Soc. Faraday Trans.* **79**, 1181–1194 (1983).
150. Levitz, P., Crespin, M. & Gatineau, L. Reduced forms of $LaNiO_3$ perovskite. 2. X-ray structure of $LaNiO_2$ and extended X-ray absorption fine-structure study — local environment of mono-valent nickel. *J. Chem. Soc. Faraday Trans.* **79**, 1195–1203 (1983).
151. Li, D. et al. Superconducting dome in $Nd_{1-x}Sr_xNiO_2$ infinite layer films. *Phys. Rev. Lett.* **125**, 027001 (2020).
152. Zeng, S. W. et al. Phase diagram and superconducting dome of infinite-layer $Nd_{1-x}Sr_xNiO_2$ thin films. *Phys. Rev. Lett.* **125**, 147003 (2020).
153. Osada, M. et al. A superconducting praseodymium nickelate with infinite layer structure. *Nano Lett.* **20**, 5735–5740 (2020).
154. Osada, M., Wang, B. Y., Lee, K., Li, D. & Hwang, H. Y. Phase diagram of infinite layer praseodymium nickelate $Pr_{1-x}Sr_xNiO_2$ thin films. *Phys. Rev. Mater.* **4**, 121801 (2020).
155. Kawai, M. et al. Orientation change of an infinite-layer structure $LaNiO_2$ epitaxial thin film by annealing with $CaH_2$. *Cryst. Growth Des.* **10**, 2044–2046 (2010).
156. Ônuki, Y., Ina, K., Hirai, T. & Komatsubara, T. Magnetic properties of intercalation compound: $Mn_{1/4}MX_2$. *J. Phys. Soc. Jpn.* **55**, 347–356 (1986).
157. Li, K. R. et al. Tunable magnetic response in 2D materials via reversible intercalation of paramagnetic ions. *Adv. Electron. Mater.* **5**, 1900040 (2019).
158. Sokolov, I. S. et al. Two-dimensional ferromagnetism in Eu-intercalated few-layer graphene. *J. Alloy. Compd.* **884**, 161078 (2021).
159. Huang, X. K. et al. Li-ion intercalation enhanced ferromagnetism in van der Waals $Fe_3GeTe_2$ bilayer. *Appl. Phys. Lett.* **119**, 012405 (2021).
160. Zheng, G. L. et al. Gate-tuned interlayer coupling in van der Waals ferromagnet $Fe_3GeTe_2$ nanoflakes. *Phys. Rev. Lett.* **125**, 047202 (2020).
161. Imanishi, N., Toyoda, M., Takeda, Y. & Yamamoto, O. Study on lithium intercalation into $MoS_2$. *Solid. State Ion.* **58**, 333–338 (1992).
162. Py, M. A. & Haering, R. R. Structural destabilization induced by lithium intercalation in $MoS_2$ and related-compounds. *Can. J. Phys.* **61**, 76–84 (1983).
163. Xiong, F. et al. Li intercalation in $MoS_2$: in situ observation of its dynamics and tuning optical and electrical properties. *Nano Lett.* **15**, 6777–6784 (2015).
164. Peng, J. et al. High phase purity of large-sized 1T′-$MoS_2$ monolayers with 2D superconductivity. *Adv. Mater.* **31**, 1900568 (2019).
165. Muscher, P. K. et al. Highly efficient uniaxial in-plane stretching of a 2D material via ion insertion. *Adv. Mater.* **33**, 2101875 (2021).
166. Brahlek, M., Koirala, N., Salehi, M., Bansal, N. & Oh, S. Emergence of decoupled surface transport channels in bulk insulating $Bi_2Se_3$ thin films. *Phys. Rev. Lett.* **113**, 026801 (2014).
167. Wang, H. T. et al. Electrochemical tuning of vertically aligned $MoS_2$ nanofilms and its application in improving hydrogen evolution reaction. *Proc. Natl Acad. Sci. USA* **110**, 19701–19706 (2013).
168. Kappera, R. et al. Phase-engineered low-resistance contacts for ultrathin $MoS_2$ transistors. *Nat. Mater.* **13**, 1128–1134 (2014).
169. Sood, A. et al. An electrochemical thermal transistor. *Nat. Commun.* **9**, 4510 (2018).
170. Gamble, F. R., Disalvo, F. J., Klemm, R. A. & Geballe, T. H. Superconductivity in layered structure organometallic crystals. *Science* **168**, 568–570 (1970).
171. Wang, C. et al. Monolayer atomic crystal molecular superlattices. *Nature* **555**, 231–236 (2018).
172. He, Q. et al. In situ probing molecular intercalation in two-dimensional layered semiconductors. *Nano Lett.* **19**, 6819–6826 (2019).
173. Wang, H. et al. Direct and continuous strain control of catalysts with tunable battery electrode materials. *Science* **354**, 1031–1036 (2016).
174. Acerce, M., Akdogan, E. K. & Chhowalla, M. Metallic molybdenum disulfide nanosheet-based electrochemical actuators. *Nature* **549**, 370–373 (2017).
175. Wan, C. L. et al. Flexible n-type thermoelectric materials by organic intercalation of layered transition metal dichalcogenide $TiS_2$. *Nat. Mater.* **14**, 622–627 (2015).
176. Wan, J. Y. et al. Tuning two-dimensional nanomaterials by intercalation: materials, properties and applications. *Chem. Soc. Rev.* **45**, 6742–6765 (2016).
177. Jung, Y., Zhou, Y. & Cha, J. J. Intercalation in two-dimensional transition metal chalcogenides. *Inorg. Chem. Front.* **3**, 452–463 (2016).
178. Yao, J. et al. Optical transmission enhacement through chemically tuned two-dimensional bismuth chalcogenide nanoplates. *Nat. Commun.* **5**, 5670 (2014).
179. Gong, Y. J. et al. Spatially controlled doping of two-dimensional $SnS_2$ through intercalation for electronics. *Nat. Nanotechnol.* **13**, 294–299 (2018). **This study combines lithographic techniques demonstrating an intercalation-based method to form in-plane heterostructures with precise size and spatial control**.
180. Bisri, S. Z., Shimizu, S., Nakano, M. & Iwasa, Y. Endeavor of iontronics: from fundamentals to applications of ion-controlled electronics. *Adv. Mater.* **29**, 1607054 (2017).
181. Rajapakse, M. et al. Intercalation as a versatile tool for fabrication, property tuning, and phase transitions in 2D materials. *NPJ 2D Mater. Appl.* **5**, 30 (2021).
182. Xue, Y. et al. Atomic-scale ion transistor with ultrahigh diffusivity. *Science* **372**, 501–503 (2021).
183. Wu, Y. et al. A two-dimensional $MoS_2$ catalysis transistor by solid-state ion gating manipulation and adjustment (SIGMA). *Nano Lett.* **19**, 7293–7300 (2019).
184. Liang, L. et al. Inducing ferromagnetism and Kondo effect in platinum by paramagnetic ionic gating. *Sci. Adv.* **4**, eaar2030 (2018).
185. Sivakumar, T. & Wiley, J. B. Topotactic route for new layered perovskite oxides containing fluorine: $Ln_{1.2}Sr_{1.8}Mn_2O_7F_2$ (Ln = Pr, Nd, Sm, Eu, and Gd). *Mater. Res. Bull.* **44**, 74–77 (2009).
186. Luneau, D., Romero, F. M. & Ziessel, R. Nitronyl nitroxide biradicals as tetradentate chelates: unusually large metal-nitroxide ferromagnetic interactions. *Inorg. Chem.* **37**, 5078–5087 (1998).
187. Almamouri, M., Edwards, P. P., Greaves, C. & Slaski, M. Synthesis and superconducting properties of the strontium copper oxy-fluoride $Sr_2CuO_2F_{2+\delta}$. *Nature* **369**, 382–384 (1994).
188. Kazakov, S. M. et al. Synthesis of alkali-substituted Sr,Cu oxycarbonates — superconductivity in $Sr_{2-x}K_xCuO_2CO_3$ ($0.25 \leq x \leq 0.7$). *Phys. C.* **253**, 401–406 (1995).
189. Ninomiya, H. et al. Calcium-free double-layered cuprate superconductors with critical temperature above 100 K. *Commun. Mater.* **2**, 13 (2021).
190. Bediako, D. K. et al. Heterointerface effects in the electrointercalation of van der Waals heterostructures. *Nature* **558**, 425–429 (2018).
191. Larson, D. T., Carr, S., Tritsaris, G. A. & Kaxiras, E. Effects of lithium intercalation in twisted bilayer graphene. *Phys. Rev. B* **101**, 075407 (2020).
192. Lu, Z. Y., Carr, S., Larson, D. T. & Kaxiras, E. Lithium intercalation in $MoS_2$ bilayers and implications for Moire flat bands. *Phys. Rev. B* **102**, 125424 (2020).
193. Wu, Y. et al. Observation of an intermediate state during lithium intercalation of twisted bilayer $MoS_2$. *Nat. Commun.* **13**, 3008 (2022).
194. Cui, X. P. et al. Rolling up transition metal dichalcogenide nanoscrolls via one drop of ethanol. *Nat. Commun.* **9**, 1301 (2018).
195. Zhao, B. et al. High-order superlattices by rolling up van der Waals heterostructures. *Nature* **591**, 385–390 (2021).
196. Gillie, L. J., Wright, A. J., Hadermann, J., Van Tendeloo, G. & Greaves, C. Synthesis and characterization of the reduced single-layer manganite $Sr_2MnO_{3.5+x}$. *J. Solid State Chem.* **167**, 145–151 (2002).
197. Lin, Z. Y. et al. Solution-processable 2D semiconductors for high-performance large-area electronics. *Nature* **562**, 254–258 (2018).
198. Cheng, S. & Wu, Z. Microfluidic electronics. *Lab Chip* **12**, 2782–2791 (2012).
199. Nguyen, P. V. et al. Visualizing electrostatic gating effects in two-dimensional heterostructures. *Nature* **572**, 220–223 (2019).



**Acknowledgements**

The authors acknowledge support from the US Department of Energy (DOE), Office of Basic Energy Sciences, Division of Materials Sciences and Engineering (Contract No. DE-AC02-76SF00515).


**Author contributions**

Researching data for article: Y.W., D.L. and C.-L.W. Review/editing of manuscript before submission: Y.W., D.L., H.Y.H. and Y.C. Substantial contribution to discussion of content: Y.W., D.L., C.-L.W., H.Y.H. and Y.C. Writing: Y.W., D.L., C.-L.W., H.Y.H. and Y.C.

**Competing interests**

The authors declare no competing interests.

**Peer review information**

*Nature Reviews Materials* thanks the anonymous reviewers for their contribution to the peer review of this work.

**Publisher's note**

Springer Nature remains neutral with regard to jurisdictional claims in published maps and institutional affiliations.